Bonding Patterns and Properties in Thermoelectric Materials

Raúl Cardoso-Gil[#], Michael Baitinger, Mitja Krnel, Frank R. Wagner and Yuri Grin[##]

Thermoelectric materials have crystal structures with a wide variety of atomic arrangements, creating intricate atomic interactions that directly affect their thermoelectric properties. In particular, heat transport properties can be better understood through knowledge of the nature of chemical bonding. The bonding patterns in intermetallic compounds and chalcogenides have been studied in order to learn more about the chemical insight into the thermoelectric properties of these materials.

Thermoelectric (TE) materials play an important role in contributing to the solutions of the global energy demand by successfully converting waste heat into useful electrical energy in power plants, homes, automobiles, space technology, etc. This realization, however, demands the development of high-performance materials based on environmentally friendly and earth-abundant constituents. The TE efficiency of any material is ruled by a dimensionless figure of merit $zT = S^2\sigma T/\kappa$, where the parameters S (Seebeck coefficient), σ (electrical conductivity), and κ [(total thermal conductivity = κ_e (electronic thermal conductivity) + κ_{lat} (lattice thermal conductivity)] are strongly intercorrelated and make it a formidable task to realize high values of zT. The only independent parameter in this equation is κ_{lat}, the reduction of which would be highly effective in triggering the overall TE performance [1]. Thus, the understanding of the nature of low κ_{lat} in crystalline materials should help in finding suitable conditions to improve their TE performance. Complex crystal structure, high atomic coordination number, high average atomic weight leading to low frequency lattice vibrations, atoms oscillating around their equilibrium position ("rattling"), increased polarity between participating atoms, enhancement of phonon scattering by lattice disorder are some of the statements found in the literature regarding the requirements to be met by potential TE compounds to achieve low thermal conductivity. The consideration of chemical aspects in the crystal structures of TE compounds, such as strong covalent interactions, bonding anisotropy and inhomogeneity, significantly strengthens our insight into the lattice thermal conductivity and, in general, into the less known chemical principles of thermoelectricity. These statements were challenging starting points for our systematic studies of different materials over the years, to learn about the nature of their properties.

As promising candidates for high temperature thermoelectric applications, intermetallic clathrates in their various types and chemical compositions were one of our first materials under study. In type-I clathrate $Ba_8Ga_{16}Ge_{30}$ the temperature dependence of the thermal conductivity shows that tunneling states play a central role in producing "phonon glass"-type thermal conductivities [2]. In $Ba_8Au_xSi_{46-x}$ (type-I) for $4.10 \le x \le 6.10$, a complex influence of Au on the thermal transport is observed, evolving from a crystalline behavior for n-type samples to a glassy one for p-type samples at high x values. In the crossover regime, a higher degree of disorder and enhanced phonon-charge carrier coupling may be at work [3]. The good TE performance of $Eu_8Ga_{16}Ge_{30}$ clathrate led to the construction of a mixed clathrate-skutterudite unicouple thermoelectric generator within a German-French-Austrian research collaboration, which produced an open circuit voltage of $U_{open} = 54$ mV and a specific electrical power of $P = 178$ mWcm^{-2} [4]. A clathrate-only TE device was developed using eight couples with the clathrates $Ba_8Ga_{16}Ge_{30}$ as n-type and $Ba_{7.8}Au_{5.33}Ge_{40.67}$ as p-type materials, which were integrated into a TE module (Figure 1), giving an output power of 0.2 W at a temperature difference $\Delta T = 380$ K ($T_1 = 673$ K and $T_2 = 293$ K) [5].

Zintl phases are also suitable for TE material development, being small band-gap semiconductors with complex crystal structures. The complexity arises from the creation of bonds between anions – i.e. the formation of polyanions – when the electron transferred from the cation is not enough to complete the valence shell of

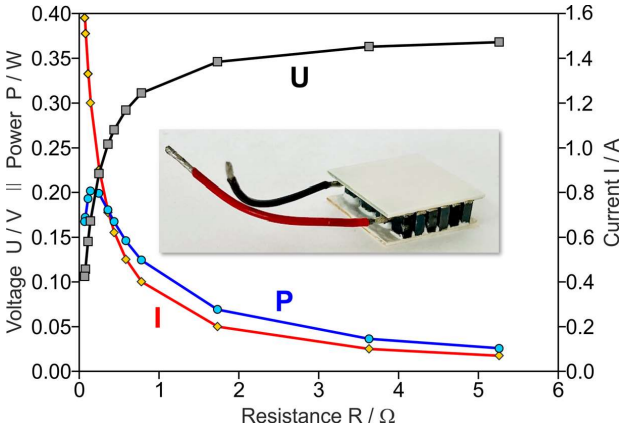

Fig. 1: Current-voltage characteristic for the chlatrate-I thermoelectric module for $T_{hot} = 673$ K and $T_{cold} = 293$ K. The electrical voltage and power share the same numerical scale with the corresponding units.

the anions. Thus, the TE properties of polycrystalline $EuZn_2Sb_2$ (space group $P\bar{3}m$) were characterized showing a high p-type Seebeck coefficient (+122 to +181 μVK^{-1}), high electrical conductivity (1137–524 Scm^{-1}), and low lattice thermal conductivity (1.60–0.40 $Wm^{-1}K^{-1}$), principally due to the low symmetry and dimensionality of the structure and the presence of heavy atoms. The obtained figure of merit reaches 0.92 at ~700°C [6]. In polycrystalline $YbCd_{2-x}Zn_xSb_2$, substitution of Cd by Zn can tune the carrier concentration and reduce thermal conductivity. For x = 0.4, the sample exhibits the highest power factor (12–20 $\mu W\ cm^{-1}K^{-2}$), the lowest lattice thermal conductivity (1.0 $Wm^{-1}K^{-1}$ at 300 K), highest zT (1.2 at 700 K). First principles calculations were performed to study the influences of bonding and electronic structures on physical properties. Only one maximum of the electron localizability indicator (ELI) is observed in the tetrahedron formed by three Sb and one Cd atom, suggesting solely four-center bonding. The whole bonding picture is, therefore, better described by the electron balance $(Yb^{2+})(Cd^{2+})_2(Sb^{3-})_2$. The more electronegative Zn^{2+} is expected to increase the covalent character of the Sb–Zn bonds, compared with the Sb–Cd bonds, leading to the narrowing of the respective bands and increasing the pseudogap depth or even opening of the real gap. This would explain the positive Seebeck coefficient and the reduced conductivity at higher Zn content [7]. Many 122-phase Zintl compounds with promising TE properties do not fulfil the given conditions of high density and complex structure on the atomic and nanoscale for TE materials with low lattice thermal conductivities. The compounds adopt three relatively simple structures with comparatively low average atomic mass, while exhibiting very low lattice thermal conductivity (κ_{lat}). Thus, the origins of low κ_L have been unveiled, where the composition, atomic arrangements, and chemical bonding play important roles in governing the phonon transport properties. The coupling between the acoustic branches and the low-frequency optical branches in a given structure results in ultralow lifetimes and sound velocities, and thus ultralow κ_L. By manipulating the chemical interactions and bonding anisotropy the phonon contribution to the total thermal conductivity would be rationally suppressed [8].

Lead telluride is a well-known thermoelectric material that undergoes a not fully understood metal–semiconductor transition at temperatures around 230°C. The temperature dependent atomic-resolution transmission electron microscopy (HRTEM) study of a single crystal reveals dislocations in the crystal structure as the cause of this effect. Shifts of atomic slabs perpendicular to {100} indicate an ordering of the stereochemically active lone pairs of lead below ~ 230°C. The local structure change causes the appearance of in-gap electronic states and leads to a metal-like electronic transport behavior. Above ~ 230°C, the dislocation disappears resulting in semiconductor-like electrical conductivity [9]. The search for materials with low lattice thermal conductivity has also focused on filled β-manganese-type phases having the chemical composition $M^{n+}_{2/n}Tr^{3+}_6Q^{2-}_{10}$ (M^{n+}: Li^+, Na^+, Ag^+, Ca^{2+}, Sn^{2+}, Pb^{2+}, Yb^{2+}; Tr^{3+}: Al^{3+}, Ga^{3+}, In^{3+}; Q^{2-}: Se^{2-}, Te^{2-}). They are characterized by close packing of Q_4-tetrahedra, analogous to the arrangement of manganese atoms in cubic β-Mn. M^{n+} ions fill all available distorted octahedral voids, and only half of them are occupied when M^{2+} ions are involved. The Tr^{3+} ions are distributed over 15% of the tetrahedral voids. These phases have large unit cells and the presence of heavy atoms suggests suitable conditions for low lattice thermal conductivity. The phases with Ca, Sn, Pb, Na, and Na/Ag exhibit very low lattice thermal conductivities. Singular crystal structural features with a three-dimensional Te-Ga network and stereochemically active lone-pair-like interactions on Te, lead to large variations in Ga-Te and

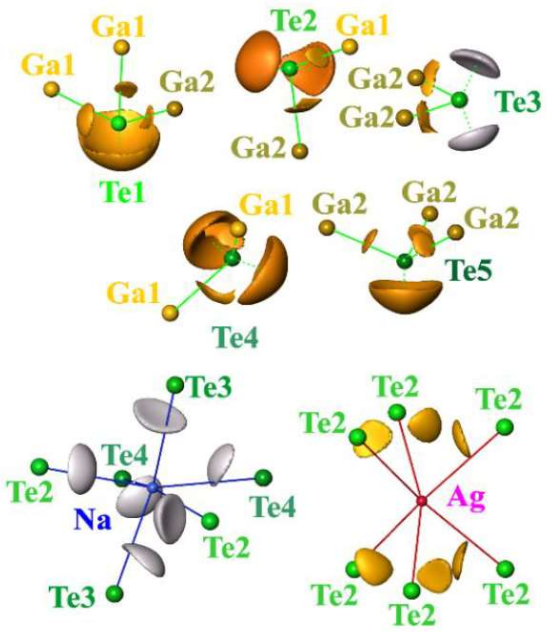

Fig. 2: (Top) ELI-D maxima isosurfaces around the Te atoms for the 3-bonded Te1, 2-bonded Te2, Te3, Te4, and 3-bonded Te5, with bold green lines showing bonding connections and the dashed green lines toward the lone-pair regions; (Bottom) tellurium environment of the sodium (blue) and silver (pink) atoms with the isosurfaces of ELI-D visualizing the lone-pair-like (strongly polar) character of bonding.

M-Te interatomic distances and large Grüneisen parameters reflecting lattice anharmonicity. The mixed cation compound $NaAgGa_6Te_{10}$ (space group *R*32) exhibits an extremely low thermal conductivity of about 0.25 $Wm^{-1}K^{-1}$ at 298 K, decreasing to 0.17 $Wm^{-1}K^{-1}$ at 773 K, which is one of the lowest values observed so far. This can be attributed to the disorder around the Na 9*d* site, described by four partially occupied sites and the stronger bonding inhomogeneity caused by the occurrence of Na-Te bonds and Ag-Te bonds with different polarities in $NaAgGa_6Te_{10}$. The analysis of the chemical bonding in position space shows two types of ELI-D maxima around the tellurium atoms (Figure 2, top). The first type of maxima is located near the Te-Ga contacts and represents the covalent bonds. The second type of maxima is located on the side of the Te atoms, where there are no Ga neighbors in the vicinity, visualizing the lone-pair-like interactions in this region. Te1 and Te5 atoms have one such region and three bonding regions – (3b)Te – while Te2-Te4 atoms have two lone-pair-like regions and two bonding regions – (2b)Te – each. The resulting pattern leads to a cumbersome thermal transport in this material and can be described by resonance phonon scattering. Due to an improved power factor as well as the ultra-low thermal conductivity, the zT value in $NaAgGa_6Te_{10}$ has been enhanced by about 4 times compared to that of the $Na_2Ga_6Te_{10}$ compound [10].

Naturally occurring chalcogenides have also drawn attention due to their interesting semiconductor properties. Phase-pure polycrystalline and mono-crystalline bournonite $PbCuSbS_3$ from mines in Neudorf im Harz, Germany and Vibora, Bolivia have been characterized by structural, chemical, spectroscopic, magnetic, and thermodynamic analyses, which confirm high quality samples for the study of intrinsic physical properties. Electronic structure calculations, electrical resistivity measurements, and spectroscopic characterizations reveal $PbCuSbS_3$ to be an n-type semiconductor with an optical energy gap E_g^{opt} = 1.69 eV as well as both a large Seebeck coefficient $S \approx -1200\ \mu VK^{-1}$ and an electrical resistivity $\rho \approx 1000\ \Omega m$ at room temperature. Bournonite has a very low thermal conductivity $\kappa(T) \approx 2–0.5\ W\ m^{-1}K^{-1}$ in the temperature range 100–600 K, dominated by optical phonons (T > 100 K), which poorly transport heat, strongly scatter the acoustic phonons, and substantially enhance the phonon-phonon *umklapp* processes. Large atomic displacement parameters and the presence of low-energy optical phonons have been identified, evidencing "rattling" effects associated to Cu and Pb atoms in the crystal structure. This leads to high Grüneisen parameters (γ_G = 4.8-3.2) and a very short phonon mean free path (l_{ph} = 11-3 Å for 100–300 K). Thus, a combination of several factors leading to large phonon anharmonicity is responsible for the low thermal conductivity in bournonite [11].

Intermetallic compounds with the formula $TMTr_3$ (*TM* = Fe, Ru, Os, Co, Rh, Ir; *Tr* = Ga, In) and a crystal structure of the $IrIn_3$ type (space group $P4_2/mnm$) have been challenging examples for the chemical understanding of the relationship between structure, bonding, and properties. The crystal structures of the $IrIn_3$ type is described as a framework built of *TM*-centered vertex-condensed tetra-capped rhombic prisms (TCRP). With the specific atomic arrangement and bonding scenario for the actual electron count, the $CoGa_3$ isoelectronic compounds should exhibit metallic conductivity while the $FeGa_3$ isoelectronic compounds present an energy gap at the Fermi level. This special feature allows band-gap tailoring by doping with non-isoelectronic substituents to tune the thermoelectric properties. Thus, for the solid solution $FeGa_{3-x}Ge_x$ with x = 0.2 an improved TE figure of merit zT_{max} = 0.21 at 765 K was obtained, with a resistivity change from semiconducting to metal-like behavior accompanied by a > 30% reduction of the thermal conductivity [12]. In $FeGa_3$, the Fe−Fe interaction represents the central point for explanation of electronic and thermal transport, as well as the optical properties of this material and its substitution variants. The required electron count of 17 ve/fu can be formally derived from eight Fe−Ga and one Fe−Fe two-center−two-electron bonds. Chemical bonding analysis in position space of $FeGa_3$ was performed on the basis of the topology of the electron localizability indicator distribution, QTAIM atoms, two- and three-center delocalization indices, domain natural orbitals, IQA analysis, and an evaluation of the Fe−Fe dissociation energy yielded a complete picture of the partially compensated Fe−Fe bond. Structural reinvestigation of differently synthesized single crystals revealed an additional occupation of empty TCRPs by Fe, depending on the preparation conditions ($Fe_{1+x}Ga_3$ with $0 \le x \le 0.018$). The additional Fe species generates in-gap states, leading to a non-vanishing density of states at the Fermi level [13]. Theoretical studies on $FeGa_3$-type representatives, $CoGa_3$ and $RhGa_3$ show no band gap, indicating metallic character, as above mentioned. However, for the isoelectronic compound $IrGa_3$ a narrow band gap of ~0.15−0.07 eV was predicted, suggesting semiconducting behavior. Single-crystal X-ray diffraction and atomic resolution TEM and STEM studies show that its real crystal structure exhibits strong local disorder with modulations in nanometer-sized regions, caused

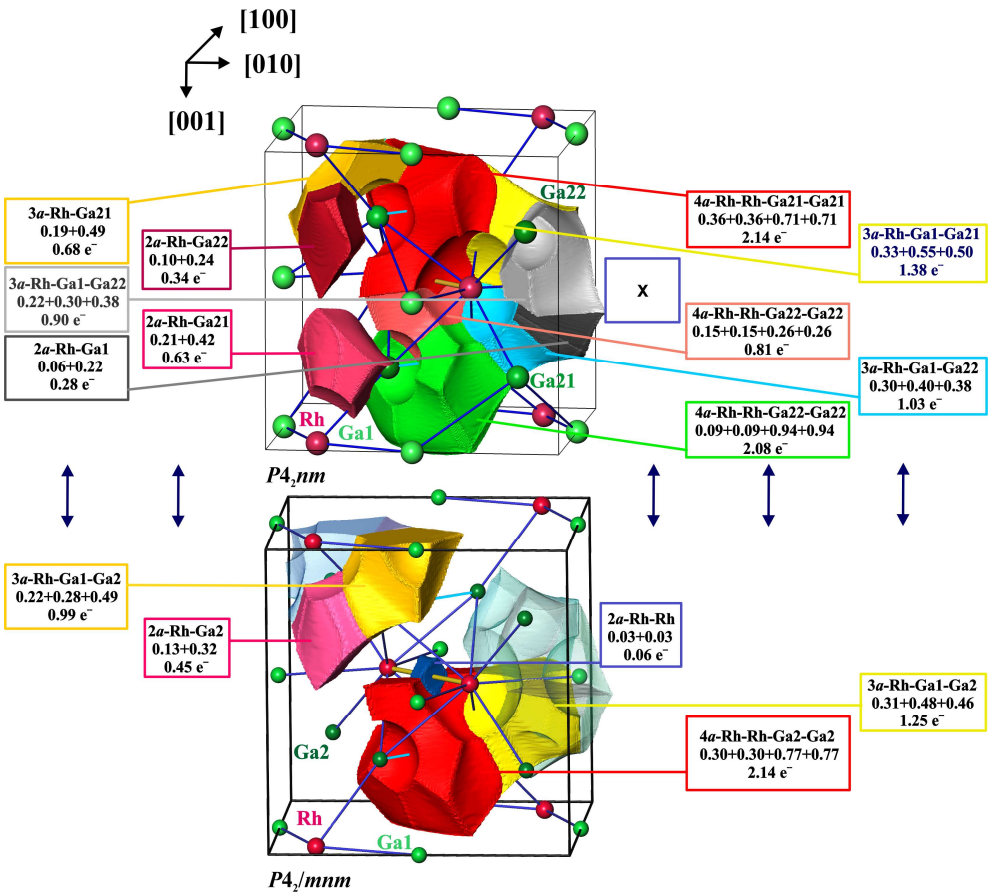

Fig. 3. Bond basins, their atomicity and electron populations in $P4_2nm$ (top) and $P4_2/mnm$ (bottom) models of the ht-Ga_3Rh crystal structure. The labels Ga21, Ga22 (top panel) and ′Ga1′, ′Ga2′ (bottom panel) denote the positions derived from the initial Ga1, Ga2 (bottom panel) by symmetry reduction.

by the ambient metastability of this high-temperature phase (existing range: $799 \leq T/°C \leq 974$). This material exhibits semiconductor-like behavior with a band gap $E_g = 0.03$ eV and a very low lattice thermal conductivity κ_{lat} (300 K) = 0.68 $Wm^{-1}K^{-1}$, attributed to the complex local atomic arrangements [14]. To complete the systematic study of the relationship between crystal structure and thermoelectric properties of Ga_3TM compounds, Ga_3Rh has been reinvestigated and the existence of two temperature-dependent modifications has been established. The high temperature modification *ht*-Ga_3Rh exists in the range $594°C \leq T \leq 792°C$. Its crystal structure can be described as a variant of the $IrIn_3$ prototype (see above) given by the 3D-arrangement of TCRPs according to $^3_\infty[Ga1_{4/2}Ga2_{8/2}Rh_2]$. Large and strongly anisotropic atomic displacement parameters of the Ga2 species in the TCRP central quadrilateral indicate critical disorder at this site, which is described by ordered low-symmetry models ($P4_2nm$, $P\bar{1}$_1 and $P\bar{1}$_2 models) yielding on average the original high-symmetry of the $IrIn_3$-type structure. The description based on ordered models allows only the study of the different atomic interactions in the disordered atomic environment. In the TCRP block $Ga1_2Ga2_4TM_2$, representing two formula units Ga_3TM, each *TM* atom is coordinated by two terminal Ga1, four bridging Ga2, two terminal Ga2 ligands, and one additional *TM* atom, resulting in a total of 17 short interatomic distances within the block. In the case of *TM* = Fe, the total number of 34 valence electrons per TCRP block is just sufficient to realize this model. In *ht*-Ga_3Rh, the additional electron given by each Rh makes the formation of the Rh-Rh bond unnecessary to satisfy the 18-electron rule. The chemical bonding studied within the position-space electron localizability approach, shows five different types of bonds by analyzing the corresponding ELI-D valence basins in the $P4_2/mnm$ model (Figure 3, bottom). With 13 bond basins per TCRP, the total number is < 17 obtained from counting the nearest-neighbor contacts because several ELI-D bond basins represent 3- and 4-atomic bonding situations. Homoatomic bonding between Rh atoms is topologically indicated in the $P4_2/mnm$ model by the presence of an ELI-D basin centered at the midpoint of the Rh–Rh internuclear line, albeit at a very low bond basin population. In a lower symmetry $P\bar{1}$_2 model, the number of different bond types is nine, larger than in the $P4_2/mnm$ model. The model accord-

ing to the space group $P4_2nm$ provides an alternative description of the splitting of the difference electron density, forming a trapezoidal shape of the central quadrilateral of the TCRP. Here, ten different bond types are observed (Figure 3, top). Rhodium participates in all heteroatomic bonds as a minority partner. A dedicated bond basin between the Rh atoms is also missing here. The bonding picture in *ht*-Ga_3Rh can be understood as a superposition of the $P4_2nm$ and the $P\bar{1}\_2$ models (mainly). While in Ga_3Fe the Fe–Fe dumbbell bonds play a key role in the bonding picture and formation of rhombic prisms, in *ht*-Ga_3Rh the decrease of the Rh–Rh bonding coupled with the increase of the Ga2–Ga2 bonding (cooperative effect) is a clear signature of the experimentally observed disorder. In agreement with the calculated electronic structure, *ht*-Ga_3Rh shows bad-metal-like temperature dependence of the electrical conductivity with electrons as charge carriers. The large atomic disorder leading to increased bond complexity – large number of different bond types – in *ht*-Ga_3Rh results in a low lattice thermal conductivity κ_{lat} (300 K) = 0.7 $Wm^{-1}K^{-1}$ of *ht*-Ga_3Rh, being comparable to that of *ht*-Ga_3Ir, and significantly lower than those of other Ga_3TM compounds with typical values greater than 3 $Wm^{-1}K^{-1}$ [15].

External Cooperation Partners

Jin-Tai Zhao (Guilin University of Electronic Technology, Guilin, China); Krzystof Wojciechowski, Oleksandr Cherniushok, Taras Parachuk (AGH University, Krakow, Poland); Roman Gumeniuk, Esteban Zuñiga-Puelles (TU Bergakademie, Freiberg, Germany).

References

[1]* *Signature Thermolelectric materials science and thecnology toward applications. K. Biswas, Z. Ren, Yu. Grin, K.-H. Lee, T. Mori, L. Chen. Appl. Phys. Lett.* ***121*** *(2022) 070401, https://doi.org/10.1063/5.0115322*

[2] *Are type-I clathrates Zintl phases and 'phonon glasses and electron single crystals'? S. Paschen, V. Pacheco, A. Bentien, A. Sanchez, W. Carrillo-Cabrera, M. Baenitz, B.B. Iversen, Yu. Grin, F. Steglich. Phys. B,* ***328*** *(2003) 39-43, https://doi.org/10.1016/S0921-4526(02)01805-7*

[3] *Low-temperature thermoelectric, galvanomagnetic, and thermodynamic properties of the type-I clathrate $Ba_8Au_xSi_{46-x}$. U. Aydemir, C. Candolfi, A. Ormeci, Y. Oztan, M. Baitinger, N. Oeschler, F. Steglich, Yu. Grin, Phys. Rev. B* ***84*** *(2011) 39-43, https://doi.org/10.1103/PhysRevB.84.195137*

[4] *A thermoelectric generator based on an n-type clathrate and a p-type skutterudite unicouple. E. Alleno, N. Lamquembe, R. Cardoso-Gil, M. Ikeda, O. Rouleau, C. Godart, Yu. Grin, Phys.Status Solidi A* ***211****, 6 (2014) 1293–1300, https://doi.org/10.1002/pssa.201300218*

[5]* *Thermoelectric characterization of the clathrate-I solid solution $Ba_{8-\delta}Au_xGe_{46-x}$. M. Baitinger, H.D. Nguyen, C. Candolfi, I. Antonyshyn, K. Meier-Kirchner, I. Veremchuk, V. Razinkov, M. Havryluk, R. Cardoso-Gil, U. Burkhardt, B. Böhme, L. Anatychuk, Yu. Grin., Appl. Phys. Lett.* ***119*** *(2021) 063902, https://doi.org/10.1063/5.0059166*

[6] *A new type of thermoelectric material, $EuZn_2Sb_2$. H. Zhang; J.-T. Zhao; Yu. Grin; X.-J..Wang; M.-B. Tang; Z.-Y. Man; H.-H. Chen. J. Chem. Phys.* ***129*** *(2008) 164713, https://doi.org/10.1063/1.3001608*

[7] *Synthesis and high thermoelectric efficiency of Zintl phase, $YbCd_{2-x}Zn_xSb_2$. X.-J. Wang; M.-B. Tang; H.-H. Chen; X.-X. Yang; J.-T. Zhao; U. Burkhardt; Yu. Grin. Appl. Phys. Lett.* ***94*** *(2009) 092106 https://doi.org/10.1063/1.3040321*

[8]* *Unveiling the origins of low lattice thermal conductivity in 122-phase Zintl compounds. K. Guo, T. Weng, Y. Jiang, Y. Zhu, H. Li, S. Yuan, J. Yang, J. Zhang, J. Luo, Y. Grin, J.-T. Zhao. Mat. Today Phys.* ***21*** *(2021) 100480, https://doi.org/10.1016/j.mtphys.2021.100480*

[9]* *Structural complexity and the metal-to-semiconductor transition in lead telluride. I. Zelenina, P. Simon, I. Veremchuk, X. Wang, M. Bobnar, W. Lu, C. H. Liebscher, Yu. Grin. Commun.Mater.* ***2*** *(2021) 99, https://doi.org/10.1038/s43246-021-00201-7*

[10]* *Lone-Pair-Like Interaction and Bonding Inhomogeneity Induce Ultralow Lattice Thermal Conductivity in Filled β-Manganese-Type Phases. O. Cherniushok, R. Cardoso-Gil, T. Parashchuk, R. Knura, Yu. Grin, K. T. Wojciechowski, Chem. Mater.* ***34*** *(2022) 6389-6401, https:// doi.org/10.1021/acs.chemmater.2c00915*

[11]* *Low thermal conductivity in bournonite $PbCuSbS_3$: A comprehensive study. E. Zuñiga-Puelles, R. Cardoso-Gil, A. Özden, N. Bulut, V. Svitlyk, C. Himcinschi, J. Kortus, R. Gumeniuk, Inorg. Phys. Rev. B* ***106*** *(2022) 195201, https://doi.org/10.1103/PhysRevB.106.195201*

[12] *Substitution Solid Solutions $FeGa_{3-x}Ex$ and Their Thermoelectric Properties. M. Wagner-Reetz, R. Cardoso-Gil, Yu. Grin. J. Electr. Mat.* ***43****, 6 (2014) 1857, DOI: 10.1007/s11664-013-2888-1, https://colab.ws/articles/10.1007%2Fs11664-013-2888-1*

[13] *On Fe−Fe Dumbbells in the Ideal and Real Structures of $FeGa_3$ F. R. Wagner, R. Cardoso-Gil, B. Boucher, M. Wagner-Reetz, J. Sichelschmidt, P. Gille, M. Baenitz, Yu. Grin, Inorg. Chem.* ***57*** *(2018) 12908−12919, https://doi.org/10.1021/acs.inorgchem.8b02094*

[14]* *The Intermetallic Semiconductor ht-$IrGa_3$: a Material in the in-Transformation State. R. Cardoso-Gil, I. Zelenina, Q. E. Stahl, M. Bobnar, P. Koželj, M. Krnel, U. Burkhardt, I. Veremchuk, P. Simon, W. Carrillo-Cabrera, M. Boström, Yu. Grin, ACS Mater. Au* ***2*** *(2022) 45−54, https://doi.org/10.1021/acsmaterialsau.1c00025*

[15]* *On chemical bonding in ht-Ga_3Rh and its effect on structural and thermoelectric behavior. R. Cardoso-Gil, M. Krnel, F. R. Wagner, Yu. Grin, Inorg. Chem.* ***63*** *26 (2024) 12156–12166, https://doi.org/10.1021/acs.inorgchem.4c01280*

[#] raul.cardoso@cpfs.mpg.de

[##] grin@cpfs.mpg.de